Journal of Colloid and Interface Science **235,** 101–113 (2001)
doi:10.1006/jcis.2000.7347, available online at http://www.idealibrary.com on IDEAL®

Spontaneous Penetration of Liquids into Capillaries and Porous Membranes Revisited

Konstantin G. Kornev[1] and Alexander V. Neimark[2]

TRI/Princeton, 601 Prospect Avenue, P.O. Box 625, Princeton, New Jersey 08542

Received May 9, 2000; accepted November 20, 2000

A critical review of the problem of spontaneous penetration of a wetting liquid into pore channels shows that no theory exists to quantitatively predict the initial stage of imbibition. Since C. H. Bosanquet (1923, *Phil. Mag.* **45, 525), the theory operates with an universal velocity $U_{\text{Bosanquet}} = (2\gamma\cos\theta/\rho r)^{1/2}$, with γ being the surface tension, θ the contact angle, r the capillary/pore radius, and ρ the fluid density. It is assumed that the initial impulse of the liquid entering the pore is insignificant for the penetration dynamics. Though the importance of the outside flow pattern has been noted in many papers, a thorough mathematical analysis of this effect is lacking in the literature. We derived a generalized equation of the fluid front motion by averaging the Euler equations of flow inside and outside the pore space. This analysis shows the significance of the flow patterns at the pore entrance. The initial stage of liquid imbibition is studied in the inviscid approximation using the methods of dynamic systems. The phase portrait of the dynamic system reveals a multiplicity of penetration regimes. Remarkably, the Bosanquet solution represents a particular regime, with the apparent mass being set zero. The Bosanquet trajectory refers to a separatrix of the phase portrait. It is shown that the initial conditions affect the rate of uptake significantly. The initial conditions stem from the prehistory of the fluid motion outside the pores prior to the liquid–solid contact. The phase portrait method allows us to distinguish two groups of solutions for the capillary rise dynamics of an inviscid fluid. The first group of trajectories corresponds to the liquid front rebound; the second group includes cyclic trajectories which correspond to the periodic regimes with liquid front oscillations at the equilibrium position. The upper estimate of the oscillation amplitude is found.**

Key Words: **liquid uptake; capillary rise; systems with variable masses; Bosanquet equation; dynamic systems; Bernoulli's oscillations.**

1. INTRODUCTION

When a capillary or a porous body is set in contact with a wetting fluid, the fluid spontaneously wets the pore walls and penetrates inside. This phenomenon is observed in many natural and physiological processes and has numerous technological applications in oil and gas recovery, civil engineering, agriculture, catalysis, paper and fiber industries, and so forth. Despite its apparent simplicity and more than 80-year history of intense studies, the problem of spontaneous penetration still attracts considerable attention and opens new challenges for physicists, chemists, and engineers (1–7).

Spontaneous liquid imbibition is caused by the forces of attraction between fluid and solid. It occurs when the free energy of the solid–gas interface exceeds the free energy of the solid–liquid interface. Therefore, wetting leads to a reduction of the total free energy of the system. An interplay of intermolecular interactions in the vicinity of the three-phase contact line gives rise to a macroscopic wetting force which depends on the surface tension of the liquid, γ, the pore radius, r, and the contact angle, θ. The latter is an effective parameter characterizing a given solid–liquid–gas system. For wetting fluids, $\theta < 90^\circ$. In cylindrical capillaries, the wetting force, expressed as the pressure difference across the liquid–gas interface, is given by the Laplace equation, $P_L = 2\gamma\cos\theta/r$. The imbibition ceases when the wetting force is balanced by an external force—in particular, gravity. The equilibrium height of the liquid rise in a capillary is given by $\ell_{\text{cap}} = 2\gamma\cos\theta/\rho g r$, with ρ being the fluid density and g the gravity.

The Lucas–Washburn Noninertial Kinetics of Uptake

Since the work of Lucas (8) and Washburn (9), the dynamics of imbibition has been described by balancing the wetting force by the gravity and the viscous Poisseuillian resistance. In so doing, the motion of the liquid column in a vertical cylindrical capillary is governed by the Lucas–Washburn (LW) equation

$$(8\eta/\rho r^2)x\,dx/dt = 2\gamma\cos\theta/\rho r - gx. \qquad [1]$$

Here, the column height is denoted by x and the fluid viscosity by η. The LW equation of the imbibition dynamics in porous solids has the same structure with effective parameters of permeability and hydraulic radius (10–12).

The LW equation has proved adequate for the uptake of viscous fluids in capillaries and porous solids of a relatively large extension in the direction of flow. Whenever the gravity factor

[1] Permanent address: The Institute for Problems in Mechanics, Russian Academy of Sciences, Prospect Vernadskogo, 101, Moscow, 117526, Russia.

[2] To whom correspondence should be addressed. E-mail: aneimark@triprinceton.org.

0021-9797/01 $35.00

is insignificant so that the inequality $x \ll 2\gamma \cos\theta/(\rho g r)$ holds, the scaling relation between the depth of penetration and time takes the form $x \sim \sqrt{t}$. Although this "diffusion" regime is well suited to the intermediate stage of imbibition in long capillaries and packed beds (11–14), the LW equation fails to describe the initial stage of penetration. Indeed, the initial velocity due to Eq. [1] is infinite, in obvious contradiction with high-resolution observations (1, 2, 6, 7, 15–21). Miller and Tyomkin, who designed a number of instruments and suggested various methods for studying spontaneous uptake experimentally, have come to the ultimate conclusion that the LW equation is inapplicable for various fibrous materials (22–24). The failure of the LW equation has been attributed to the neglect of fluid inertia.

"Inertial Capillarity"

While the idea of accounting for the fluid inertia looks trivial, the approach to "inertial capillarity" (1) is not so simple as it seems at a first sight. The key question concerns the form of the equation describing the motion of liquid column. Particularly, the terms associated with the effect of attachment/detachment of fluid particles at the capillary entrance have been attracting a long-lasting continuous discussion in the literature (1, 6, 10–30).

Indeed, the problem of the correctness of the ordinary Newtonian equation governing the capillary rise kinetics has been posed long ago, back in the 18th century. We thank G. K. Mikhailov (26) for pointing us to the letter from Georg Wolfgang Krafft to Euler (dated September 24, 1748) in which Kraft had put forward the puzzle:

> The mechanical rule $dc = p\,dt/m$ or $c\,dc = p\,ds/m$ assumes that the mass m is constant during the entire motion; would it not be possible to create such a rule in which the mass, or rather the moving point, could be variable? . . . I think that it would then become possible to derive the measure of the rise of fluids into capillary tubes, for in this case the mass that rises increases all the time. Please, Sir, let me know your thoughts regarding this matter at some suitable opportunity.

The Euler answer is unavailable; most likely, it did not survive (26). This historic excursus shows that the problem of capillary rise represents an instructive example of the motion of a system of variable mass. Typical for such systems, uncertainty concerns the momentum flux flowing in/out of the moving liquid column when the fluid particles are attached to or detached from it (31–33). There are two distinct points of view on the role of outside flow: some researchers believe that the outside flow is unimportant while others consider the outside effects crucial for the initial uptake dynamics.

The Kinetics Unaffected by the Outside Flow Pattern: The Bosanquet Equation

Almost 200 years after Krafft's letter and 2 years after the Washburn publication (9), Bosanquet considered the capillary rise dynamics by ignoring the flow outside the capillary entrance (29). He showed that the effect of fluid inertia modifies the LW equation to give

$$d(x\,dx/dt)/dt + (8\eta/\rho r^2)x\,dx/dt = 2\gamma\cos\theta/\rho r - gx. \quad [2]$$

At the initial stage of liquid penetration the inertial and capillary forces dominate the others:

$$d(x\,dx/dt)/dt \approx 2\gamma\cos\theta/\rho r. \quad [3]$$

Assuming that the initial momentum of liquid is zero, $x\,dx/dt = 0,\ t = 0$, Bosanquet come to a finite initial penetration velocity given by

$$U_{\text{Bosanquet}} = \sqrt{\ell_{\text{cap}}\mathrm{g}} = (2\gamma\cos\theta/\rho r)^{1/2}. \quad [4]$$

Thus, accounting for fluid inertia remedies the velocity divergence inherent to the LW equation. The Bosanquet velocity is *universal*: It is independent of the conditions of penetration. However, initial velocities observed in high-resolution uptake experiments were found to be finite, yet different from this universal value (1, 6, 15–21); see Section 2 for details.

The Kinetics Influenced by the Outside Flow Effects: The SNC Equation

The next principal step in understanding the problem of spontaneous penetration was taken by Szekely *et al.* (30). They coupled the outside and inside hydrodynamics and considered the effect of apparent mass caused by the flow pattern outside the capillary. The authors modified the Bosanquet equation [2] by introducing the apparent mass in the form

$$d((x + cr)\,dx/dt)/dt + (8\eta/\rho r^2)x\,dx/dt = 2\gamma\cos\theta/\rho r - gx, \quad [5]$$

where c is a constant of the order of unity ($c = 7/6$ in the original paper (30)). In the Szekely–Neumann–Chuang (SNC) equation [5], the initial velocity is set to zero ($dx/dt = 0,\ x = 0,\ t = 0$), and, therefore, it is implied that the initial acceleration is finite and given by $d^2x/dt^2 = 2\gamma\cos\theta/c\rho r^2$ at $x = 0,\ t = 0$. It is worth noting that similarly to the Bosanquet approach, in the SNC approach, the initial momentum of the liquid column is neglected ($x\,dx/dt = 0$ at $x = 0, t = 0$), which leaves no room for a consistent consideration of the effects of the outside flow development. The correct formulation of the initial conditions is crucial if, for example, one attempts to distinguish between the dynamics of absorption of a droplet impinging upon a sheet of writing paper and that of a droplet gently deposited on a paper towel.

Thus, the existing models of liquid imbibition operate with three initial velocities: infinite (LW equation), zeroth (SNC equation), and universal (Bosanquet equation).

Paper Outline

This paper is aimed at a revision of the fundamentals of the theory of liquid uptake. We start from a critical review of experimental data on spontaneous liquid penetration and show that the zeroth initial velocity implied by the SNC model is not justified (Section 2). The Bosanquet velocity [4] was never observed as well, yet it gives a rough estimate of the initial velocity either for low-viscosity liquids or for sufficiently wide capillaries.

Thus, the treatment of experimental data corresponding to the inertial regime of liquid imbibition is questionable. To resolve this contradiction, we have derived the equation of capillary rise of an inviscid fluid, augmenting the SNC equation. The approach is based on averaging the Euler equations inside and outside the pore space (Section 3). We show that various hydrodynamic schemes of fluid flow at the capillary inlet lead to distinct flow regimes (Section 4). Using the method of phase portraits, we analyze the SNC equation and reveal a wide spectrum of solutions, which are determined by initial conditions associated with apparent mass and reactive impulse of the fluid column (Section 5). The flow pattern at the inlet not only affects the rate of liquid uptake, but also influences the maximal rise of the meniscus. The method proposed describes also the oscillating regime of imbibition of inviscid liquids observed recently by Querre (1) (Sections 4, 5). In this paper, we focus on the problem of the correct description of the moving front during the capillary rise. We implicitly assume the applicability of a one-dimensional approach, ignoring 3D flow patterns at the pore entrance and at the meniscus. Dynamic contact angle effects and associated problems of meniscus formation are also neglected. These problems are poorly understood, yet existing practice (1, 15, 17) shows that the time of meniscus formation is much less than the time scale under consideration. Although beyond the main scope of this paper, the question will be briefly addressed under Discussion.

2. EXPERIMENTAL OBSERVATIONS

The flow visualization experiments and measurements of the rate of liquid uptake are restricted mainly to the channels of simplest geometries, the Hele–Shaw cells (21), and axisymmetric capillaries (1, 6, 17, 19, 20). The results of these observations are summarized in Table 1. In most of the experiments, a regime with a finite initial velocity was observed. However, its magnitude was always smaller than the Bosanquet velocity [4].

In the microgravity experiments (21), a Hele–Shaw cell with an encapsulated drop was released from a height of 110 m in an evacuated container with the internal pressure below 1 mbar. The free fall time was about 5 s. Practically weightless conditions ($10^{-5}\,g$) were reached within few milliseconds. Due to a rapid change of acceleration from the normal gravity to microgravity, the liquid was forced to fill the Hele–Shaw cell. The dynamics of liquid invasion was recorded and the dynamics of the liquid finger propagation was evaluated. Two different regimes of liquid propagation were observed depending on the fluid viscosity. In the case of viscous fluids (3M Fluorinert Dielektrika FC-77, viscosity 0.013–0.015 ps), the liquid front propagated upward as the square root of time (LW kinetics), while in the case of low-viscosity fluids (dimethylsiloxane polymers, viscosity $\sim$0.005 and $\sim$0.0078–0.009 ps) the liquid front moved with a constant velocity appreciably different from the Bosanquet value (see Table 1). Since the detailed rheological properties of these fluids are unavailable, a quantitative analysis is hindered.

TABLE 1
Results of the Liquid Uptake Experiments

Liquid	Viscosity, η (mPa-s)	Density, ρ (kg/m^3)	Surface tension, γ (mN/m)	Capillary radius, r (10^{-6}m)	Kinetics	Equilibrium height, $\ell_{cap} = 2\cos\theta \times \gamma/\rho g r$ (mm)	Bosanquet velocity, $U_{Bosanquet} = \sqrt{\ell_{cap} g}$ (cm/s)	Observed velocity (cm/s)
Silicone oil[a]	0.5×10^3	980	21.1	421	Lucas–Washburn	10.4	31	$\div$
Ethanol[a]	1.17	780	21.6	689	Bosanquet-like	8.1	28	17 ± 1
Ethanol[b]	1.17	780	21.6	242	Bosanquet-like	23.2(24.2)	47.8(48.8)	15.5
Ether[a]	0.3	710	16.6	689	Oscillations observed	7.1	26	23
Mixture[c]	0.77	955	57	2500	Bosanquet-like	4.8	2	3
Water[d]	1	998	71.8	133	Bosanquet-like	110	104	30
Water[d]	1	998	71.8	298	Bosanquet-like	49	69	47
Water[d]	1	998	71.8	420.5	Bosanquet-like	35	58	39
Water[d]	1	998	71.8	595.5	Bosanquet-like	24.6	49	35
Water[b]	1	998	71.8	242	Bosanquet-like	60	77	$15 \div 14$
Water[b]	1	998	71.8	285	Bosanquet-like	51	71	$18 \div 20$

[a] Quere (1), $\theta = 0^\circ$.
[b] LeGrand and Rense (15), $\theta = 0^\circ$.
[c] Sell *et al.* (19), $\theta = 10^\circ$.
[d] Jeje (17), $\theta = 0^\circ$, vertical and horizontal orientation of capillaries.
[e] Since in (15) and (17) the physical properties of water and ethanol used were not reported, we took the standard values at room temperature. The data in the parentheses correspond to the measured values.

Qualitatively similar results were obtained by Sell *et al.* in 1984 (19) and Sell and Maisch in 1986 (20). The authors traced the liquid column movement and the meniscus shape in microgravity experiments. A mixture of cyclohexane and carbon tetrachloride in softened water was used. The liquid rise in glass tubes was filmed at 200 frames/s. The menisci observed in space deviated from the hemispherical shape and were less stable than those observed on Earth. The authors argued that hydrodynamic forces cause the meniscus shape deformation.

A number of experiments were performed in capillaries of various shapes, including unduloidal, cone-like, and sinusoidal channels. Several researchers used glass capillaries of different sizes to study the dynamics of capillary rise by stroboscopic photography (time intervals of 1/10 and 1/20 s (15)) and by high-speed camera (500–2000 images per second (17); 200 images per second (1, 6)).

Quere (1) reported instructive results on capillary rise of various wetting fluids. For high-viscosity fluids such as silicone oil, the height of the liquid column followed the Lucas–Washburn kinetics ($x \approx \sqrt{t}$) at short time intervals (with the resolution $\approx$1 image per 0.4 s) and, when approaching ℓ_{cap}, the column height relaxed exponentially with the characteristic relaxation time $\tau_\eta = 16\gamma\eta\cos\theta/(\rho^2 g^2 r^3)$. Almost inviscid fluids such as ethanol and ether showed a different kinetics. In particular, within the initial time interval up to 20 ms when the ethanol column traveled about 3 mm, the relation between the column height and time was linear. Remarkable results were obtained as the liquid viscosity decreased so that the time of viscous reaction became smaller than the characteristic time of liquid uptake. This condition ensures the applicability of the inviscid fluid approximation. The time of viscous reaction can be estimated by setting the corresponding Reynolds number to the order of unity, $\tau_{\text{Re}} = \rho r^2/8\eta$. In other words, it is assumed that within this time interval both terms in the LHS of Eq. [2] are of the same order of magnitude. Omitting the outside flow effects, the characteristic time of liquid uptake can be roughly assessed as $\tau_{\text{Bosanquet}} = \ell_{\text{cap}}/U_{\text{Bosanquet}}$. In terms of viscosity, the condition of validity of the inviscid fluid approximation, $\tau_{\text{Re}} \gg \tau_{\text{Bosanquet}}$, is given by the constraint $\eta \ll g\rho^{3/2} r^{5/2}(2\gamma\cos\theta)^{-1/2}/8$. In this case, Quere observed power descending oscillations, $h \propto 1/t$, of the liquid column near the equilibrium position, instead of the exponential relaxation. A reasonable explanation of the oscillation regime was given recently in (6). However, as we show below (see Section 5), the oscillations of an inviscid fluid are largely affected by the outside flow patterns.

As seen in Table 1, the initial velocity of liquid uptake is finite, in contradiction with the SNC model, but does not follow the Bosanquet law [4]. The measured velocity is systematically lower than the Bosanquet value [4] and depends on the physicochemical properties of the liquid as well as on the experimental conditions. However, the tendency toward the Bosanquet velocity [4] can be revealed from the Quere experiments (1) on ether and from the Jeje data (17) also. It is worth noting that the SNC approach can be applied either (*i*) at the immediate vicinity of the moment of meniscus formation or (*ii*) when the developed flow pattern has been settled. The intermediate regime of flow at the pore entrance cannot be described within the inviscid fluid approximation. In the first case, the physical picture is akin to the sudden detachment of a rigid disk from the liquid surface. Specifically, while the disk takes up some velocity, the liquid in the container is still motionless due to its inertia (34). In the second case, for applicability of the inviscid fluid approximation, the meniscus has to travel some distance from the capillary end to avoid the problems of meniscus/capillary edge hydrodynamic interactions. Most likely, the experimentalists observed the second case, because the cameras used were unable to trace all the events from the uptake beginning. If so, the Jeje observation (17) of a tendency for the initial velocities to be close to the Bosanquet value [4] can be explained by sufficiently wide capillaries employed. Indeed, as the capillary radius increases, the contribution of the viscous forces to the force balance decreases compared with the inertial forces. In fact, the Bosanquet and SNC regimes are characterized by a well-developed core flow with a thin lubricating viscous boundary layer. This flow pattern is seemingly kindred to that existing at Borda's mouthpiece (34). Assuming that the camera traced the events shifted from the uptake onset, one may ignore the effect of the apparent mass to get a rough estimate of the initial velocity. In such a case the Bosanquet value gives a reasonable upper estimate for the initial velocity in accord with the experimental trend.

From this brief review of the available experimental data we conclude that neither of the models proposed earlier can describe a finite initial velocity of uptake and oscillating relaxation of the liquid front at the equilibrium position. Both these phenomena, more prominent for low-viscosity fluids, are related to the coupling of the inside and outside flow patterns. Below, we propose a generalized model of uptake dynamics in the inviscid fluid approximation and elucidate a general form of the equation of capillary rise and rebound.

3. DERIVATION OF THE BASIC MODEL FOR A SINGLE CAPILLARY

Consider a capillary immersed vertically into a container filled with an incompressible liquid (Fig. 1). The flow is described by the Euler equation

$$\rho\frac{\partial \mathbf{u}}{\partial t} = -\nabla\cdot\pi, \qquad [6]$$

where $\mathbf{u}$ is the fluid velocity and π is the stress tensor. In order to derive the equation of the meniscus motion, let's integrate the X-component of Eq. [6] over the volume V occupied by the fluid. The volume V is limited by the container walls and the moving surfaces: the meniscus in the capillary and the free surface of the bulk liquid outside the capillary. These surfaces

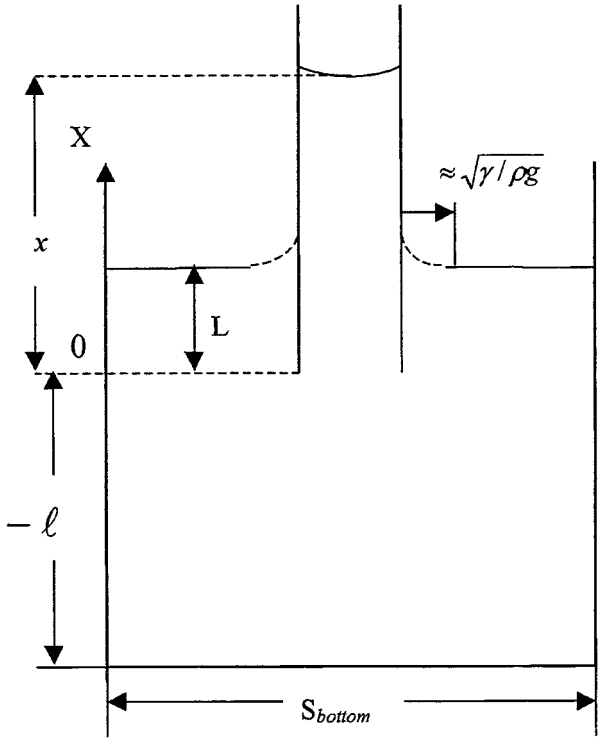

FIG. 1. Schematic of capillary rise experiment.

are moving in opposite directions. The integration gives

$$\rho \int_V \frac{\partial u_X}{\partial t}\, dV = -\int_V \nabla_i \pi_{iX}\, dV. \qquad [7]$$

The RHS can be transformed into the surface integral

$$-\int_V \nabla_i \pi_{iX}\, dV = -\oint_S n_i \pi_{iX}\, dS, \qquad [8]$$

where **n** is the external normal to the surface, and S is the surface of the fluid boundary. Restricting ourselves to the case of inviscid fluids, we can write the components of the stress tensor as (34)

$$\pi_{ik} = \delta_{ik} p + \rho u_i u_k + \rho g X \delta_{iX} \qquad i, k = x, y, z. \qquad [9]$$

Up to this point, we have used the basic hydrodynamic equations. No specific features of the process have been utilized. Based on specific conditions of experiments, the customary assumptions allow us to simplify the calculations (30). It is worth noting that, in general, the free surface outside the capillary is not absolutely flat, but is slightly bent at the capillary wall. However, if the container size is much larger than the characteristic length of a capillary wave, $\sqrt{\gamma/\rho g}$, the contribution of this region into the surface integral [8] is negligible. Therefore, we can use the following kinematic conditions for the velocity at the free surfaces:

$$u_X|_{\text{at the meniscus}} = \dot{x},$$
$$u_X|_{\text{at the free surface outside the capillary}} = \dot{L}. \qquad [10]$$

Accounting for the assumed uniformity of the pressure distribution over the free surfaces, the surface integral [8] is reduced to

$$\begin{aligned} -\oint_S n_i \pi_{iX}\, dS &= -\oint_S (n_X p + \rho u_X \mathbf{u}\mathbf{n}\, dS - \rho g n_X X)\, dS \\ &= -p(L)(S_{\text{bottom}} - S_{\text{capillary}}) - p(x) S_{\text{capillary}} \\ &\quad - \rho \dot{L}^2 (S_{\text{bottom}} - S_{\text{capillary}}) - \rho \dot{x}^2 S_{\text{capillary}} \\ &\quad - \rho g L (S_{\text{bottom}} - S_{\text{capillary}}) - \rho g x S_{\text{capillary}} \\ &\quad + \int_{S_{\text{bottom}}} p(-\ell)\, dS, \end{aligned} \qquad [11]$$

where $-\ell$ is the X-coordinate of the container bottom. Assuming that the container is much larger than the immersed part of the capillary, the flow can be considered localized at the capillary entrance. Therewith, the pressure field outside the immediate vicinity of the capillary entrance is hydrostatic, and we can set for the pressure at the container bottom $p(-\ell) = p_{\text{atmospheric}} + \rho g(L + \ell)$. Making use of the incompressibility condition

$$L = (V_0 - (x + \ell) S_{\text{capillary}})/(S_{\text{bottom}} - S_{\text{capillary}}), \qquad [12]$$

where V_0 is the initial fluid volume, and applying the Laplace equation for the pressure difference across the meniscus, Eq. [11] can be simplified to

$$\begin{aligned} -\oint_S n_i \pi_{iX}\, dS &= \frac{2\gamma \cos\theta}{r} S_{\text{capillary}} - \rho \dot{x}^2 S_{\text{capillary}} [1 + S_{\text{capillary}}/ \\ &\quad (S_{\text{bottom}} - S_{\text{capillary}})] - \rho g (x + \ell) S_{\text{capillary}} \\ &\quad \times [1 + S_{\text{capillary}}/(S_{\text{bottom}} - S_{\text{capillary}})] \\ &\quad + \rho g V_0 S_{\text{capillary}}/(S_{\text{bottom}} - S_{\text{capillary}}). \end{aligned} \qquad [13]$$

Consider now the LHS of Eq. [7]. Following the above assumptions, it is convenient to rewrite the time derivative as

$$\begin{aligned} \rho \int_V \frac{\partial u_X}{\partial t}\, dV &= \rho \frac{d}{dt} \int_V u_X dV - \rho \dot{L}^2 (S_{\text{bottom}} - S_{\text{capillary}}) \\ &\quad - \rho \dot{x}^2 S_{\text{capillary}} \approx \rho S_{\text{capillary}} \frac{d}{dt}[x\dot{x}] \\ &\quad + \frac{d}{dt} \int_{V_{\text{container}}} u_X\, dV - \rho \dot{x}^2 S_{\text{capillary}} \\ &\quad \times [1 + S_{\text{capillary}}/(S_{\text{bottom}} - S_{\text{capillary}})]. \end{aligned} \qquad [14]$$

Comparing Eqs. [13] and [14], we arrive at the basic equation

$$\rho S_{\text{capillary}} \frac{d}{dt}[x\dot{x}] + \rho \frac{d}{dt} \int\limits_{V_{\text{container}}} u_X \, dV = -\rho g S_{\text{capillary}}[1 + S_{\text{capillary}}/(S_{\text{bottom}} - S_{\text{capillary}})](x - x_0), \quad [15]$$

where

$$x_0 = [V_0/(S_{\text{bottom}} - S_{\text{capillary}}) + \ell_{\text{cap}}]/[1 + S_{\text{capillary}}/(S_{\text{bottom}} - S_{\text{capillary}})] - \ell. \quad [16]$$

As seen, Eq. [16] cannot be reduced to the Bosanquet form as the ratio $S_{\text{capillary}}/(S_{\text{bottom}} - S_{\text{capillary}})$ diminishes. We need also to put ($l = V_0/(S_{\text{bottom}} - S_{\text{capillary}})$. Even in such a limit, the equation contains an extra term, which is determined by the flow pattern outside the capillary inlet. This term can be treated as a reaction force of the outside fluid

$$F_{\text{reaction}} = -\rho \frac{d}{dt} \int\limits_{V_{\text{container}}} u_X \, dV, \quad [17]$$

or the "net rate at which positive momentum flows in" the capillary (30). (See also (31–33) for historical review of various approaches to treatment of systems with variable mass.)

4. EFFECT OF THE FLOW PATTERN ON THE REACTION FORCE

As discussed by Quere *et al.* (6), the dynamics of upward and downward front motion are different. First, let us show the distinguishing features of the upward and downward motion, restricting ourselves to potential flows, $\mathbf{u} = \nabla\varphi$.

Sink/Source Flow Patterns

In upward motion, the outside flow looks like a sink flow (Fig. 2a) or the flow at Borda's mouthpiece: the fluid underneath the pore entrance is involved in the upward motion without eddies (if the capillary edges are suitably designed (1, 34)). Due to the assumption that the fluid at the container bottom is motionless, the potential diminishes there, so that $\varphi \to 0$, $X \to -\ell$. The reaction force Eq. [17] can be written as

$$F_{\text{reaction}} = -\rho \frac{d}{dt} \int\limits_{S - S_{\text{capillary}}} \varphi(L) \, dS - \rho \frac{d}{dt} \int\limits_{S_{\text{capillary}}} \varphi(0) \, dS. \quad [18]$$

As an illustration, we may consider the case of an impacting capillary, $L = 0$. Mathematically, this problem is equivalent to determining the irrotational flow due to an impact of a rigid disk of radius r (34). Using the solution to this problem (34), we get

$$F_{\text{reaction}} = -\frac{4r\rho}{3\pi} \ddot{x} S_{\text{capillary}}.$$

Thus, we arrive at the SNC equation [5] with the apparent mass $\rho c r S_{\text{capillary}} = 4\rho r S_{\text{capillary}}/(3\pi)$. In other words, the fluid volume involved in such a motion is of the order of the volume of the sphere with the radius equal to the capillary radius. Considering another limiting case of a developed sink-type flow, the authors of (30) obtained another estimate, $c = 7/6$. Both these results are expected from a dimensional analysis. Indeed, the only length scale associated with the source type flow is the capillary radius. Therefore, the apparent mass cannot depend on another scale.

Recirculatory Flows

The outside flow patterns during the outward front flow may be significantly different from the sink/source flow patterns (see (35, 36) for reviews). Zauner (35) observed two typical flow schemes. If the Reynolds number is large (in the Zauner experiments on glycerol jets $\text{Re} = 2Vr\rho/(\eta\sqrt{6}) = 30$, where V is the volumetric mean velocity obtained from the flow-rate measurements), the flow pattern is akin to that of the source flow. In this case, one can expect the apparent mass of the same order of magnitude as that for the sink-flow pattern. As the Reynolds number decreases (below 10 in the Zauner experiments on glycerol jets), a toroidal eddy is observed (Fig. 2b). As explained by Schneider, this complex flow is caused by the fluid viscosity (see review (36) and references therein). To see what kind of modifications of the SNC equation might be expected, let us simplify the picture. First, integration of the X-velocity component over the regions containing the viscous toroidal eddy and the wakes behind it gives rise to a negligibly small term. In other words, we can assume that the fluid particles are stirred immediately after they reach these regions. The particles mostly drift in the planes of the fluid table but not transversally. Thus, the major contribution to the reaction force comes from the region of the jet branching (Fig. 2c). Entering the motionless fluid, the jet disperses to form an umbrella-like shell. The shell shape changes along with the variation of the jet discharge. Treating the jet flow within the inviscid approximation and accounting for the above simplifications, the reaction force can be represented as

$$\rho \frac{d}{dt} \int\limits_{V_{\text{jet region}}} u_X \, dV = \rho \oint\limits_{S_{\text{jets}}} u_n u_X \, dS = \rho \int\limits_{S^+_{\text{jet}}} u_n u_X \, dS - \rho \int\limits_{S^-_{\text{jet}}} u_n u_X \, dS. \quad [19]$$

Here S_{jet} is the whole jet surface consisting of the upper S^+_{jet}

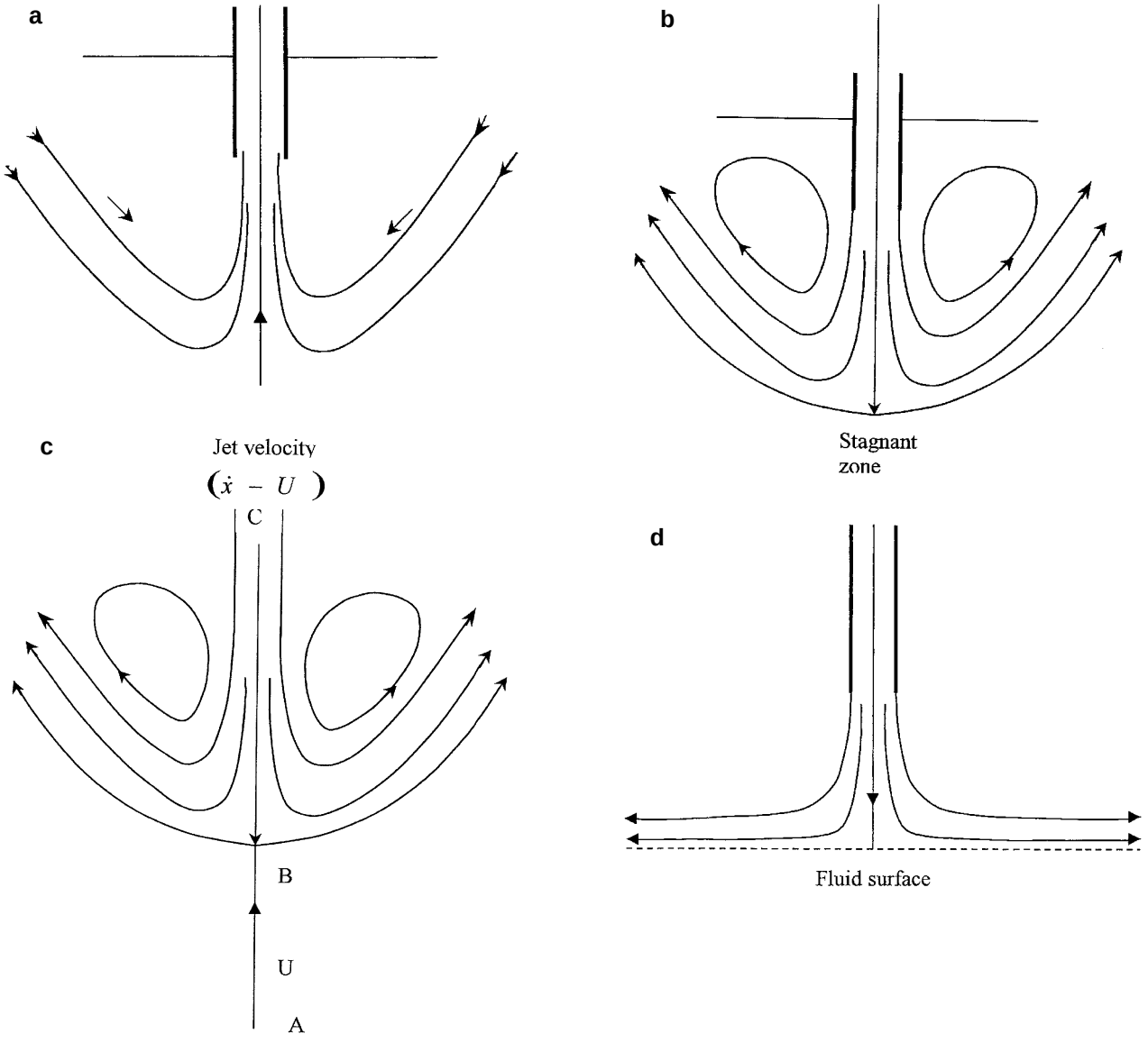

FIG. 2. Characteristic features of the flows at the capillary entrance: (a) Sink-type flow pattern, (b) Recirculatory flow. (c) The model of a jet penetrating stagnant zone steadily. In the frame moving with the penetration velocity U, the umbrella-like contours are fixed. (d) A limiting case of jet penetration when the fluid surface keeps its planar unperturbed configuration.

and lower S^-_{jet} umbrella surfaces. In thin-layer approximation, both umbrella sides look like equidistant surfaces; therefore, the RHS of Eq. [19] can be calculated to give

$$\rho \int_{S^+_{\text{jet}}} u_n u_X \, dS - \rho \int_{S^-_{\text{jet}}} u_n u_X \, dS \approx -\rho S_{\text{cap}} U^2, \qquad [20]$$

where U is the velocity of the jet branching point B in Fig. 2c, which can be called the jet penetration velocity (37, 38). The latter differs from the velocity of meniscus, but is of the same order of magnitude. Indeed, assuming the process to be steady, we can apply Bernoulli's theorem to the axial streamline ABC—precisely, to the points A and C. Disregarding the pressure difference from the hydraulic thrust, we get $(\dot{x} - U)^2 = U^2$ or $U = \dot{x}/2$ (37).

Thus, modeled as a stagnant zone, the eddies confine the fluid flow into a jet bounded by free surfaces. The fluid behind the jet head is motionless. At each instant of time it can be imagined as a curvilinear rigid wall. The jet flow at the branching point looks like that observed when a jet impinges upon a curvilinear cavern. Invading the motionless fluid, the jet undergoes a fluid reaction referred as a ricochet effect. Thus, the recirculatory flow is responsible for the additional reaction force.

The presence of the fluid surface could affect the curvature of the jet streamlines, and, therefore, could alter the jet propagation velocity as well. Hence, the anticipated form of the reaction force in the recirculatory flow regime is

$$F_{\text{reaction}} = -\frac{d}{dt}\int\limits_{V_{\text{container}}} u_X\, dV = \chi\rho S_{\text{capillary}}\dot{x}^2. \qquad [21]$$

Bernoulli's Oscillations

It is worth noting that the model recently suggested in (6) to explain the observed oscillations of the liquid front implies Eq. [21] with $\chi = 1$. In our model, this is a limiting situation, which corresponds to jet spreading over the fluid surface without penetration underneath (Fig. 2d). In other words, the fluid surface serves as a rigid reflecting substrate (34). As the fluid particle reaches the capillary exit, the velocity vector immediately turns perpendicularly. Thus, $\chi = 1$ is the upper limit corresponding to a maximal possible effect of the streamline folding.

The problem of column rebound in a capillary is equivalent to column fall in a tube due to gravity, which deserved special attention in the classical Bernoulli's "Hydraulics" dating back to 1738 (25). Bernoulli considered a columnar motion in which a pipe, full of a heavy inviscid fluid, is put in contact with a pool of the same fluid. The pipe radius was assumed to be large relative to the capillary length, so that the capillary effects had been ignored. Neglecting the flow outside the pipe, but assuming that "the particles of fluid flowing out fall within the ambient liquid immediately after discharge and then diffuse from here," Bernoulli showed that the motion of the fluid column upward differs from the downward motion. In the modern language, the energy dissipation due to viscosity has been attributed to the change of kinetic energy, in accord with the suggestion of Quere *et al.* (6). The explanations of the capillary rise oscillations and the corresponding equations for the maximal and minimal values of the column positions are similar to those obtained by Bernoulli for gravity-driven flow in a pipe (25).

Porous Membrane

Distinct from single capillaries, the outside flow patterns during the capillary rise and rebound in a porous membrane are expected to be of the sink/source kind. Considering a porous membrane as a bundle of capillaries, one can be convinced that a well-developed recircular flow at each pore entrance is unlikely, because a system of jets coming to or emanating from the pores makes the stream laminar. The characteristic length associated with the outside flow is much greater than the pore size. To support this idea, we recall that the problem of the outside flow is akin to the problem of disc impact (34). But for the latter it is known (34) that the order of magnitude of the disc apparent mass is that of a sphere with a radius comparable to the membrane size.

Generalized Equation of the Liquid Front Motion

Summarizing the results, we conclude that in the limit of a negligible capillary radius,

$$S_{\text{capillary}}/(S_{\text{bottom}} - S_{\text{capillary}}) \to 0, \qquad [22]$$

the generalized equation of the front motion in the inviscid fluid approximation can be written as

$$d((x + cr)\,dx/dt)/dt - \chi(dx/dt)^2 = 2\gamma\cos\theta/\rho r - gx. \qquad [23]$$

In many cases the recirculatory flow does not develop ($\chi = 0$), and Eq. [23] reduces to the SNC equation [5] for an inviscid fluid. Equation [23] describes the front motion at intermediate Reynolds numbers, with $\chi = 0$ for upward motion, and with $c = 0$, $0 < \chi \le 1$ for downward motion.

The SNC equation can be justified by averaging the Euler equation assuming that the flow at the capillary entrance is of the sink/source kind. This assumption is applicable only if the Reynolds number is large enough. Unfortunately, the specific values of the admissible Reynolds numbers are unavailable for the case when the free fluid surfaces are present in the container. We can refer only to the experiments with fluids in confined boxes (34, 35). The rate at which the outward column carries out the momentum cannot be expressed in a uniform form for the whole range of Reynolds numbers. Therefore, neither phenomenological equations suggested in (27) nor equations from (28) can be justified. For large Reynolds numbers we can use the SNC equation, while for the Reynolds numbers compatible for the ricochet regimes of column fall, the column rise and fall must be considered differently (6, 25).

In the next section we present a detailed analysis of the SNC equation for an inviscid fluid to reveal the possibility for getting a better description of the uptake data within its framework. The oscillating regimes will be discussed briefly, only to enrich the scheme offered in (6).

5. ANALYSIS OF THE SNC MODEL

Below, we classify all possible regimes of the capillary uptake dynamics allowed by the SNC equation [5] for an inviscid fluid, $\eta = 0$. Assume that the capillary just touches the free surface, $L = 0$, and the capillary radius is much smaller than the container cross-sectional area. Scaling the front position by the equilibrium capillary length, $H = x/\ell_{\text{cap}}$, and the time by the characteristic time, $\tau = \sqrt{\ell_{\text{cap}}/g}$, $T = t/\tau$, we arrive at the dimensionless equation

$$d((H + \alpha)\,dH/dT)/dT = 1 - H, \qquad [24]$$

where $\alpha = cr/\ell_{\text{cap}}$.

It is convenient to rewrite this equation as a dynamic system:

$$(H + \alpha)\,dH/dT = Z, \qquad [25]$$

$$dZ/dT = 1 - H. \qquad [26]$$

The fist line is merely the definition of the momentum of a system with variable mass, and the second line expresses the force balance.

General Properties of the Dynamic System [25] and [26]

The system [25] and [26] allows us to perform a complete analysis of the problem using the phase portrait method of classical mechanics. In particular, one can be convinced that the only stationary point of this system is $(Z_{st}, H_{st}) = (0, 1)$. The vertical line $H = -\alpha$ is a special line at which the velocity dH/dT changes sign. Moreover, in the point $(0, -\alpha)$, the velocity is undetermined. Linearization of the system [24] and [25] in the vicinity of the special points (Z_{st}, H_{st}) and $(0, -\alpha)$ shows that the first point is elliptic, while the second is hyperbolic. The elliptic stationary point corresponds to the equilibrium position of the meniscus, $H_{st} = 1, dH/dT/_{H_{st}=1} = 0$. In the vicinity of the equilibrium position the meniscus oscillates. Scanned in variables (Z, H), the oscillations form elliptic streamlines. The physical meaning of the hyperbolic point is not so obvious.

Using the first integral,

$$dZ^2/2 = (H + \alpha)(1 - H)\,dH, \qquad [27]$$

one can parameterize all the streamlines of the dynamic system by the integration constant C as

$$Z^2/2 = H^2(1 - \alpha)/2 - H^3/3 + \alpha H + C. \qquad [28]$$

Qualitatively different solutions of the dynamic system [25] and [26] are separated by the *separatrix* which consists of the loop and two branches emerging from the hyperbolic special point $(0, -\alpha)$ (Fig. 3). The separatrix loop intersects the axis $Z = 0$ at $H = -\alpha$ (the hyperbolic special point) and at $H = H_s$ (the most right point of the separatrix). The value of H_s is given by

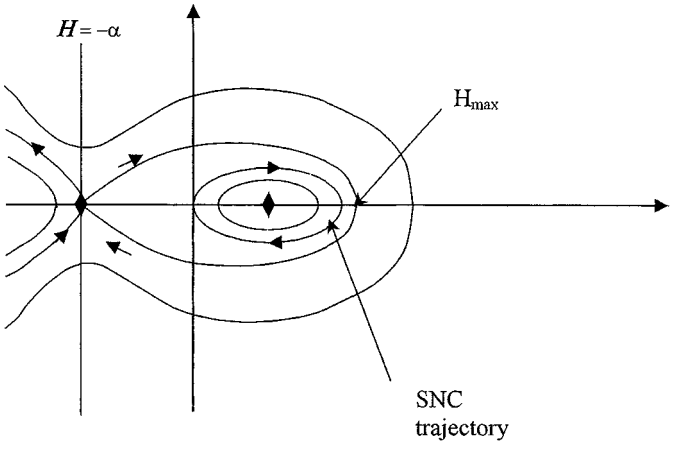

FIG. 3. Phase portrait of the dynamic system [24]–[25]. SNC is the Szekely–Neumann–Chuang solution. The symbols ♦ denote the stationary points of the system.

the solution to the algebraic equation

$$H_s^2(1 - \alpha)/2 - H_s^3/3 + \alpha H_s + \alpha^3/6 + \alpha^2/2 = 0. \qquad [29]$$

The separatrix is specified by the value of $C = C_s = \alpha^3/6 + \alpha^2/2$. If $C > C_s$, we have two families of the streamlines that start/end at the vertical line $H = -\alpha$. The streamlines of the first family located to the right of the vertical line $H = -\alpha$ envelop the separatrix loop and intersect the axis $Z = 0$ at $H > H_s$,. The streamlines of the second group located to the left of the vertical line $H = -\alpha$ have no physical meaning. They are going monotonically to/from minus infinity, $H \to -\infty$. If $C < C_s$, we have another two families of the streamlines. Within the separatrix loop there are the cyclic trajectories enveloping the stationary point (Z_{st}, H_{st}). Inside the curved corner formed by the separatrix branches at $H < -\alpha$, the **U**-shaped streamlines can be imagined as produced by a vortex at the left infinity.

Physical Meaning of the Solutions

Each trajectory including the separatrix corresponds to a particular solution of the equation [24] specified by given initial conditions. Therewith, only those trajectories that intersect the Z-axis and are located in the right half-plane $H > 0$ are physically meaningful as related to the problem of spontaneous uptake. Among them, the cyclic trajectory—which contains the origin of coordinates ($H = 0$, $Z = 0$)—corresponds to the zeroth initial velocity as prescribed by the SNC approach. In the inviscid approximation considered here, the cyclic SNC trajectory corresponds to the oscillations of the liquid front around the equilibrium height with complete bounce back to the pore entrance. The others trajectories envelop the SNC trajectory and correspond to nonzeroth initial velocities, $dH/dT = Z/\alpha > 0$ at $H = 0$. According to these trajectories the liquid injected with a nonzeroth velocity will pass the equilibrium height, achieve a maximum, rebound, and leave the capillary. This behavior is predicted for an ideal inviscid fluid. In real situations, even low viscosity causes the transformation of the cyclic trajectories in the phase portrait (Fig. 3) into the spiral trajectories reeling in the stationary point $H = H_{st}$. However, for any viscosity there exists a value of the initial injection velocity above which the complete rebound is possible.

The cyclic trajectories inside the SNC loop refer to another physical experiment. Assume that the liquid front initially equilibrated in the capillary at $H = H_{st}$ is forced to retract by applying an external pressure. When the applied pressure is released, the liquid front returns back to the equilibrium height. Is this case, one would observe oscillations around the equilibrium.

The right pole of the SNC trajectory determines the maximal height of the oscillating liquid column, H_{max}, that is given by the first integral [28] at $C = 0$:

$$H_{max}^2 - \frac{3}{2}H_{max}(1 - \alpha) - 3\alpha = 0 \qquad \text{or}$$

$$H_{max} = \frac{3}{4}(1 - \alpha) + \sqrt{\frac{9}{16}(1 - \alpha)^2 + 3\alpha}. \qquad [30]$$

Remarkably, the dimensional maximal height $x_{\max}$ is always smaller than the doubled capillary length, $2\ell_{\text{cap}}$. As the dimensionless apparent mass α tends to zero, the maximal height approaches $3\ell_{\text{cap}}/2$ as shown in (1), and only when the apparent mass tends to infinity the maximal height asymptotically reaches $2\ell_{\text{cap}}$. The latter case can be attributed to a porous membrane, for which the characteristic length scale for outside flow is associated with the thickness of the fluid penetration.

Energy Considerations

The authors of (6) posed a question of why the energy apparently is lost. Indeed, if one derives the equation of motion by applying the hypothesis of energy conservation, the resulting equation will differ from Eq. [25]. In the limiting case $\alpha \to 0$, the solution gives $H_{\max} = 2$ instead of $3/2$ (6). This puzzle is typical for all problems in which the mass of the system does vary (31–34, 39). In fact, the energy F of moving liquid column can be expressed as a sum of the kinetic energy T and the potential energy E, $F = T + E$. Using the first integral [28], this sum can be evaluated to give

$$F = T + E = \frac{\dot{Z}^2}{2(H+\alpha)} + \frac{1}{2}H^2 - H = \frac{1}{6}\frac{H-3}{H+\alpha}H^2. \quad [31]$$

It is apparent that the energy is lower than the initial potential energy attributed to $H = 0$ (Fig. 4). The energy loss in an inviscid fluid is not an artifact of the theory. It is merely a consequence of the mass variability in this particular system. In the whole fluid filling the capillary and container, energy is conserved (see for details some discussions of open and closed mechanical systems in (31–33)). As seen from Eq. [31], the front will move until the energy reaches its minima. The condition for energy minima is

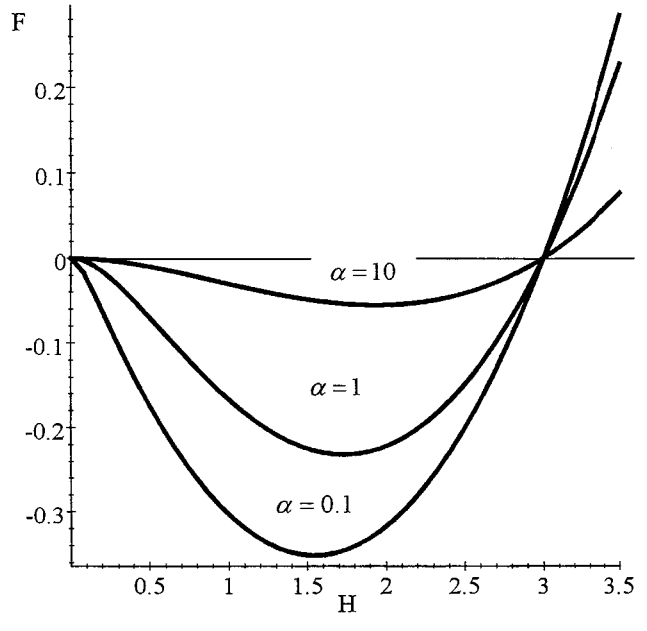

FIG. 4. The energy as a function of the front position for various dimensionless apparent masses.

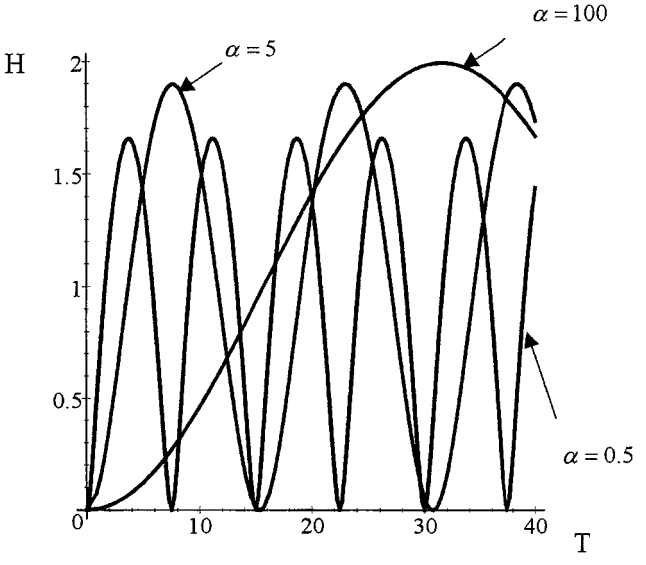

FIG. 5. The dimensionless column height as a function of the dimensionless time for various dimensionless apparent masses.

expressed by Eqs. [30]. The period of oscillations for the SNC solution can be found by direct integration of [28] assuming $C = 0$. The latter allows us to extract two limiting asymptotes. As the apparent mass tends to zero, we get the period $T = 6$ (1), and in the opposite case, $\alpha \to \infty$, we have $T \propto \sqrt{\alpha}$. In Fig. 5, the SNC solution is plotted for various dimensionless apparent masses.

In summary, the SNC solution describes the spontaneous rise of liquid front from $x = 0$ to $x = \ell_{\text{cap}} H_{\max}$ and backward rebound to $x = 0$. Affected by the apparent mass, the maximal height varies in the range $3/2 < H_{\max} < 2$ as the dimensionless apparent mass increases from zero to infinity.

It should be noted that the cycles in the phase plane are transformed into spirals if we account for the fluid viscosity. In other words, the periodic oscillations are damped. Though an analysis of the viscosity effects lies beyond the scope of this paper, in Fig. 6 we plot sample curves, which typify the dynamics of fluid uptake for various regimes. The viscosity parameter $\Omega = 8\tau_{\text{Bosanquet}}/\tau_{\text{Re}}$ characterizes the effect of fluid viscosity as discussed in Section 2. The condition for front oscillations can be found from the SNC equation [5] linearized about the equilibrium solution $H = 1 + \varepsilon$, $\varepsilon \ll 1$. Written in a dimensionless form, the criterion for the oscillation regime relates the viscosity parameter Ω and the apparent mass α as $\Omega \le 2(1+\alpha)$. Thus, the effect of apparent mass extends the range of viscosity admissible for oscillations (6). Within this range, the fluid uptake is mostly controlled by the inertial and capillary forces. As seen from typical Fig. 6, the inviscid fluid approximation works quite well within almost the whole time interval of the first rise.

The Bosanquet Solution

As discussed above, the inviscid approximation [24] describes the initial stage of liquid penetration until the viscosity effects

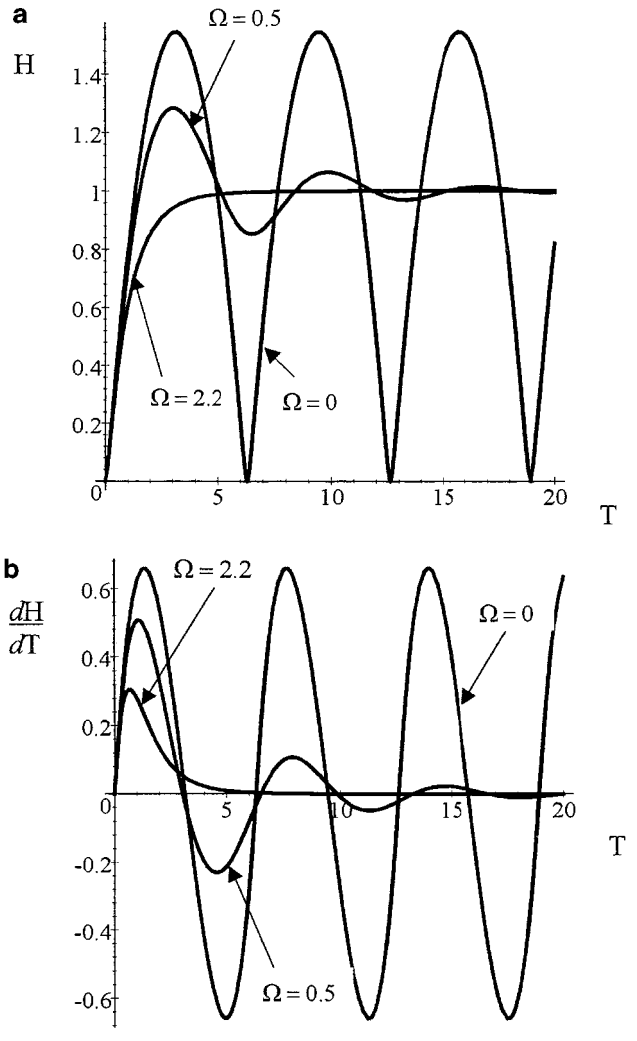

FIG. 6. The effect of fluid viscosity. (a) The dimensionless column height as a function of the dimensionless time for various Ω. (b) The dimensionless velocity of front propagation as a function of the dimensionless time. The dimensionless apparent mass is $\alpha = 0.1$. The upper border for existence of front oscillations corresponds to $\Omega = 2.2$.

become comparable to the inertial ones. Thus, the phase portrait in Fig. 1 shows that for any initial injection velocity there exists a solution. The zeroth initial velocity assumed in the SNC approach is not exceptional. It is interesting to analyze how the proposed analysis is related to the Bosanquet approach, which implies a finite universal initial velocity. To make this comparison, one must let $\alpha \to 0$. However, the transition to this limit is not straightforward.

Decreasing the magnitude of α to zero, one arrives at the situation when the line $H = -\alpha$ merges with the line $H = 0$. Therewith, the origin of coordinates is transformed into the hyperbolic special point and the loop of separatrix replaces the cyclic SNC trajectory. The cyclic trajectories inside the loop of separatrix refer to the oscillations around the equilibrium and are qualitatively similar to the cyclic trajectories inside the SNC trajectory for nonzeroth α's.

However, although the trajectories enveloping the loop of separatrix retain their nonsingular topological shape as α tends to zero, the corresponding solutions alter their behavior significantly. Each of these solutions is characterized by a finite nonzeroth momentum $Z = H\,dH/dT = C \neq 0$ at $T = 0$. As seen from Eq. [28], when $\alpha = 0$ and $H \to 0$, the liquid front advances as $H \sim T^{1/2}$, implying $dH/dT \to \infty$, but this "diffusion" kinetics is physically different from the LW regime. This regime is caused by an intricate momentum balance at the initial instant of liquid penetration. The momentum $Z = H\,dH/dT$ cannot be set to zero, rather it depends on the dynamics of the fluid pattern development outside the pore at the moment of the first liquid–solid contact. This effect is seemingly kindred to the rocket jet effect. Indeed, although there is no visible movement at the moment of start, the jet impulse forces the rocket to take off. Thus, in general, one has to set a nonzeroth momemtum $Z = C \neq 0$ at $T = 0$ as an initial condition for the Bosanquet equation [3]. Since the viscous forces on the initial stage of penetration are dominated by the inertial ones, the same arguments regarding the effect of a nonzeroth initial momentum are applicable in a general situation of viscous fluid uptake.

Consider the singular solution corresponding to the loop of separatrix, for which the initial momentum is zero, $Z = 0$ at $T = 0$. This trajectory is the Bosanquet solution. Indeed, using the first integral [28] with $C = C_s = \alpha^3/6 + \alpha^2/2$ in the limit of vanishing α,

$$\lim_{\alpha\to 0} U_\alpha = \lim_{\alpha\to 0} dH/dT|_{\text{separatrix},\,H=0} = \lim_{\alpha\to 0} \frac{1}{\alpha}\sqrt{\alpha^3/3 + \alpha^2} = 1, \qquad [32]$$

we arrive in the dimensional variables at the Bosanquet characteristic velocity $U_{\text{Bosanquet}} = dx/dt|_{x,t=0} = \sqrt{\ell_{\text{cap}} g}$. Thus, the transition from the general equation [24] to the Bosanquet equation in not analytical. Although small, the term associated with α gives rise to a singular perturbation of the solution and is responsible for the initial kinetics of uptake.

Mechanical Analogies

There is a very helpful mechanical analog of the Bosanquet problem that allows us to look at the problem from another point of view (31–33, 39). Consider an ideally flexible uniform heavy chain initially coiled at the table. If it is pulled up by a constant force numerically equal to our wetting force, the motion of its head end can be found by integrating Eq. [24] with $\alpha = 0$. At each time new links are attached to the bottom end by *inelastic shocks* caused by impulse $2\pi r\gamma \cos\theta\, dt$. The change of momentum of the end element dx due to this shock is $\pi r^2 \rho U_{\text{Bosanquet}}\, dx$. Equating both increments, we arrive at the Bosanquet velocity. The energy in such a motion is not conserved, but a part is lost due to the shocks. The effect is apparent if we consider the inverse motion, when the chain is falling down. For this process we have

the Meshcherskii equation of motion (32, 33, 39, 40) in which the reaction of the substrate has to be included into the force balance $x\,d^2x/dt^2 = F_{\text{reaction}} - (dx/dt)^2 + 2\gamma\cos\theta/\rho r - xg$. The reaction force can be found by considering the momentum balance at the chain end as above, $F_{\text{reaction}}\,dt = (dx/dt)\,dx$. Therefore, we have the equation

$$x\,d^2x/dt^2 = 2\gamma\cos\theta/\rho r - xg, \qquad [33]$$

which is exactly the equation suggested in (6). As mentioned before, the same equation was introduced by Bernoulli to describe the fall of a fluid column in a pipe (25).

Although useful, the analogy with the chain motion cannot be extended directly onto the hydrodynamic problem without a thorough hydrodynamic justification. In the general case of a nonzeroth α, the initial velocity is expressed via the Bosanquet value and a prefactor $u = \sqrt{2C/\alpha^2}$ as

$$dx/dt|_{x=0} = uU_{\text{Bosanquet}} = \sqrt{2\ell_{\text{cap}}gC/\alpha^2}. \qquad [34]$$

Thus, the solution characterized by $C = \alpha^2/2$ gives the initial velocity equal to the Bosanquet value. If $C > \alpha^2/2$, the initial velocity is greater than the Bosanquet value; otherwise it is smaller.

6. DISCUSSION AND CONCLUSIONS

The above analysis allows us to look at the discrepancy between the Bosanquet–Szekely–Neumann–Chuang theories and experimental data on spontaneous uptake from a different point of view. According to Eq. [24], the penetration regimes are determined by the dimensionless factor $\alpha \approx r/\ell_{\text{cap}}$ (c is assumed to be of the order of unity). In so doing, the initial velocity is specified by the integration constant C, Eq. [34]. In the experiments (Table 1) with the linear Bosanquet-like kinetics, the observed initial velocity was smaller than the Bosanquet value. Hence, the corresponding solutions of the SNC Eq. [24] are characterized by the integration constant $C < \alpha^2/2$. The experimental observation, however, cannot be proved on the basis of the mathematical model in Eqs. [25] and [26]. The model under consideration does not impose any restriction on the range of admissible initial velocities.

Although justified for applications at the length scales much greater than the pore size, the SNC approach requires an accurate formulation of the initial conditions. The initial velocity of liquid penetration is determined by the conditions of the liquid–solid contact. It depends on the process prehistory and the specifics of adhesion interactions. While the hydrodynamic factor associated with a particular fluid flow pattern outside the pore space is intuitively understandable (liquid can be delivered to the pore entrance with different velocities), the adhesion factor is not so obvious and has not yet received a proper consideration. A detailed discussion of the contact conditions of the liquid–solid bridging will be presented elsewhere. The origin of the adhesion effect is as follows. When a liquid–gas interface approaches a solid surface, it inevitably enters the region of action of intermolecular forces. For a van der Waals fluid, the solid–liquid intermolecular interactions become dominant when the gap width narrows to about 1 μm. Once this distance is approached, the solid surface pulls up the liquid–gas interface to form a bridge. Further, the bridge spreads over the solid and the liquid invades the pore space. That is, even under the conditions of an initially flat undisturbed liquid surface and a vanishing relative velocity of the liquid–solid approach, the adhesion effect gives rise to a nonzeroth rate of the initial liquid invasion. A solution of the bridging problem would provide a startup impulse of the invading liquid, which should be accounted for in the initial conditions to the SNC equation. The hydrodynamic problem of bridging is akin to the classical problem of the impact of a body on a free surface of liquid (34). Another problem beyond the scope of the paper concerns the meniscus formation. To be consistent, we have to assume that the time of the meniscus formation is much smaller than the hydrodynamic time $\tau = \sqrt{\ell_{\text{cap}}/g}$. The problem of the first approach and the problem of meniscus formation are interconnected and their solution is highly desirable.

In summary, we conclude that the generalized equation of uptake in the inviscid approximation [23] allows one to consider a variety of regimes of spontaneous liquid penetration characterized by different initial velocities. There are two groups of solutions: One corresponds to the liquid rebound. The other describes the periodic regimes characterized by the liquid front oscillations around the equilibrium position. The inviscid approximation is suitable for analyses of the initial stage of uptake while the viscosity effects are insignificant. The consideration of viscous dissipation at the later stage of uptake would lead to the deterioration of liquid oscillations. The developed method extends the area of applicability of the conventional theories, such as the Bosanquet and Szekely–Neumann–Chuang models, which are restricted to the assumption that the fluid invades the pore with a vanishing impulse. The initial conditions of liquid penetration are affected by the outside hydrodynamic effects and the solid–liquid adhesion interactions.

ACKNOWLEDGMENTS

We thank I. Tyomkin for numerous illuminating discussions, D. Quere for valuable comments on the initial version of this paper, and G. K. Mikhailov for sending us references to the classical works on the mechanics of the systems with variable masses. The work was supported by a group of TRI/Princeton corporate members.

REFERENCES

1. Quere, D., *Europhys. Lett.* **39,** 533 (1997).
2. Siebold, A., Walliser, A., Nardin, M., Oppliger, M., and Schultz, J., *J. Colloid Interface Sci.* **186,** 60 (1997).
3. Ugarte, D., Stockli, T., Bonard, J. M., Chatelain, A., and de Heer, W. A., *Appl. Phys. A* **67,** 101 (1998).
4. Schaffer, E., and Wong, P.-Z., *Phys. Rev. Lett.* **80,** 3069 (1998).
5. Davis, S. H., and Hocking, L. M., *Phys. Fluids* **11,** 48 (1999).

6. Quere, D., Raphael, E., and Ollitrault, J.-Y., *Langmuir* **15,** 3679 (1999).
7. Siebold, A., Nardin, M., Schultz, J., Walliser, A., and Oppliger, M., *Colloids Surf. A* **161,** 81 (2000).
8. Lucas, R., *Kolloid Z.* **23,** 15 (1918).
9. Washburn, E. W., *Phys. Rev.* **17,** 273 (1921).
10. Kheifetz, L. I., and Neimark, A. V., "Multiphase Processes in Porous Media," Khimia, Moscow, 1982.
11. Akselrud, G. A., and Altschuler, M. A., "Introduction to Capillary–Chemical Technology," Khimia, Moscow, 1983.
12. Bear, J., "Dynamics of Fluids in Porous Media," Dover, New York, 1988.
13. Dullien, F. A. L., "Porous Media: Fluid Transport and Pore Structure," 2nd. ed. Academic Press, New York, 1992.
14. Quere, D., DiMeglio, J. M., Brochard-Wyart, F., *Rev. Phys. Appl.* **23,** 1023 (1988).
15. LeGrand, E. G., and Rense, W. A., *J. Appl. Phys.* **16,** 843 (1945).
16. Siegel, R., *J. Heat Transfer* **28,** 165 (1961).
17. Jeje, A. A., *J. Colloid Interface Sci.* **69,** 420 (1979).
18. Letelier, S. M. F., Leutheusser, H. J., and Rosas, Z. C., *J. Colloid Interface Sci*. **72,** 465 (1979).
19. Sell, P. J., Maisch, E., and Siekmann, J., *Acta Austronaut.* **11,** 577 (1984).
20. Sell, P. J., and Maisch, E., *Acta Austronaut.* **13,** 87 (1986).
21. Dreyer, M., Delgano, A., and Rath, H. J., *J. Colloid Interface Sci*. **163,** 158 (1994).
22. Miller, B., and Tyomkin, I., *Text. Res. J.* **54,** 706 (1984).
23. Miller, B., Tyomkin, I., and Friedman, H. L., "Book of Papers, INDA-TEC 94, Baltimore, September 1994," p. 133, Association of the Nonwoven Fabrics Industry, New York, 1994.
24. Tyomkin, I., and Miller, B., *in* "Proceedings of the Absorbent Products Conference, October, 1994," X-1, Marketing/Technology Service, Charleston, South Carolina, 1994.
25. Bernoulli, D., and Bernoulli, J., "Hydrodynamics and Hydraulics," Dover, New York, 1968.
26. Quotation from G. K, Mikhailov, "Introduction," *in* D. Bernoulli, "Werke. Bd. 5, *Hydrodynamik*," (G. K. Mikhailov, Ed.) Basel e.a. Birkhäuser, in press.
27. Menon, V. J., and Agrawal, D. C., *Am. J. Phys.* **55,** 63 (1987).
28. Duarte, A. A., Strier, D. E., and Zanette, D. H., *Am. J. Phys.* **64,** 413 (1996).
29. Bosanquet, C. H., *Phil. Mag.*, Ser. 6 **45,** 525 (1923).
30. Szekely, J., Neumann, A. W., and Chuang, Y. K., *J. Colloid Interface Sci*. **35,** 273 (1971).
31. Tiersten, M. S., *Am. J. Phys.* **37,** 82 (1969).
32. Mikhailov, G. K., *Mekh. Tverd. Tel.* **5,** 11 (1975).
33. Mikhailov, G. K., *Bull. IMA* **20,** 13 (1984).
34. Batchelor, G. K., "An Introduction to Fluid Dynamics," Cambridge Univ. Press, Cambridge, UK, 1967.
35. Zauner, E., *J. Fluid. Mech.* **154,** 111 (1985).
36. Schneider, W., Zauner, E., and Bohm, H., *Trans. ASME, J. Fluid Eng.* **109,** 237 (1987).
37. Birkhoff, G., MacDougall, D. P., Pugh, E. M., and Taylor, G., *J. Appl. Phys.* **29,** 563 (1948).
38. Birkhoff, G., and Caywood, T. E., *J. Appl. Phys.* **20,** 646 (1949).
39. Panovko, Ya. G., "Solid Mechanics: Modern Concepts, Confusions and Paradoxes," Nauka, Moscow, 1985.
40. Meshcherskii, I. V., "Dynamics of a Point with Variable Mass," St. Petersburg, 1897.